EDITORIAL CSIC

Materiales de Construcción
76 (361) January-March 2026, e399
ISSN-L: 0465-2746, eISSN: 1988-3226
https://doi.org/10.3989/mc.2026.414925

ARTICLE

Impact of ZnO and TiO_2 on C-S-H composition and its correlation with antifungal properties in cement pastes

Impacto de ZnO y TiO_2 en la composición del gel C-S-H y su correlación con las propiedades antifúngicas en pastas de cemento

F. Amor
Laboratory of Applied Materials Chemistry, Center of Materials Science, Faculty of Sciences, Mohammed V University, (Rabat, Morocco), Department of Building Structures, Faculty of Civil Engineering, Czech Technical University in Prague, (Prague, Czech Republic)
Corresponding author: fouad.amor@fsr.um5.ac.ma, https://orcid.org/0000-0001-7517-4652

H. Agourrame
Laboratory of Applied Materials Chemistry, Center of Materials Science, Faculty of Sciences, Mohammed V University, (Rabat, Morocco)
hind.agourrame@gmail.com, https://orcid.org/0000-0002-8794-0702

Z. Racova
Department of Building Structures, Faculty of Civil Engineering, Czech Technical University in Prague, (Prague, Czech Republic)
zuzana.racova@fsv.cvut.cz, https://orcid.org/0000-0003-1245-5769

N. Khachani
Laboratory of Applied Materials Chemistry, Center of Materials Science, Faculty of Sciences, Mohammed V University, (Rabat, Morocco)
n.khachani@um5r.ac.ma, https://orcid.org/0000-0001-5041-0081

P. Hajek
Department of Building Structures, Faculty of Civil Engineering, Czech Technical University in Prague, (Prague, Czech Republic)
petr.hajek@fsv.cvut.cz, https://orcid.org/0000-0003-2389-9306

Abstract: This study presents a self-cleaning cement incorporating zinc oxide and titanium dioxide nanoparticles, used alone or in combination. The objective is to develop high-performance materials suitable for different environments, inhibiting fungal growth while providing self-cleaning properties. In parallel, the impact of these nanoparticles on the mineralogy and structure of C-S-H was examined. Used as partial cement substitutes (0–3% by weight), the pastes were characterized after 28 days of hydration by XRD, XRF, DSC and TG to evaluate reactivity and Ca/Si ratios of the formed C-S-H. Next, a new alternative method for the indirect determination of the Ca/Si ratio of the C-S-H gel in cements is also proposed using three methods. The antimicrobial surfaces were assessed for antifungal activity against *Penicillium brevicompactum, Trichoderma reesei and Aspergillus niger* on Czapek-Dox agar. Results show that the addition of TiO_2 and ZnO yields fungal-resistant surfaces, promoting hygiene, sustainability and innovation in construction.

Keywords: Nanoparticles; ZnO; TiO_2; Antifungal; Cement hydration; C-S-H; Ca/Si ratio.

Resumen: *Este estudio presenta un cemento autolimpiante con nanopartículas de óxido de zinc y dióxido de titanio, usadas solas o combinadas. El objetivo es desarrollar materiales de alto rendimiento que inhiban el crecimiento de hongos y aporten propiedades autolimpiantes. Se evaluó además el efecto de estas nanopartículas en la mineralogía y la estructura del gel C-S-H. Empleando estas nanopartículas como sustitutos parciales del cemento (0–3 % en peso), las pastas se caracterizaron tras 28 días de hidratación mediante XRD, XRF, DSC y TG*

para analizar la reactividad y la relación Ca/Si del gel C-S-H. También se propone un método alternativo para determinar de forma indirecta la relación Ca/Si del gel en cementos a través de tres enfoques. Las superficies antimicrobianas se ensayaron contra Penicillium brevicompactum, Trichoderma reesei y Aspergillus niger en agar Czapek-Dox. Los resultados confirman que la incorporación de TiO_2 y ZnO genera superficies resistentes a hongos, favoreciendo higiene y sostenibilidad en la construcción.

Palabras clave: Nanopartículas; ZnO; TiO_2; Antifúngico; Hidratación del cemento; C-S-H; Relación Ca/Si.

Received: 24-04-2025 / **Accepted**: 04-03-2026 / **Published**: 08-06-2026

Citation: Amor F, Agourrame H, Racova Z, Khachani N, Hajek P. 2026. Impact of ZnO and TiO_2 on C-S-H composition and its correlation with antifungal properties in cement pastes. https://doi.org/10.3989/mc.2026.414925

Supplementary information ↓

1. INTRODUCTION

Cement is a particularly complex system to characterize, both in terms of its chemical composition and crystalline structure, as well as the morphology of the solid phases formed during its hydration. To date, the characterization of cement hydrates, in particular hydrated calcium silicates, remains a challenge despite the numerous research projects carried out in this field (1). Hydrated calcium silicates (C-S-H) are formed by the hydration of silicates present in clinker and constitute between 60 and 70% of the total volume of the hydrated cement paste. Essential elements of Portland cement, they play a major role in its properties, in particular by ensuring a large part of its mechanical strength (2).

The composition of C-S-H is generally described from the CaO/SiO_2 ratio noted Ca/Si and the calcium hydroxide concentration at equilibrium (3). Most of the work carried out on this hydrate suggests the existence of several C-S-H of different stoichiometry, structure or morphology (3–5). All of these studies agree to demonstrate that the variation of the stoichiometry composition of C-S-H in terms of Ca/Si ratio varies with the concentration of CaO in solution in which it is in equilibrium. Thus, the higher the concentration of CaO, the higher the Ca/Si ratio of C-S-H (6). In hydrated calcium silicates, the Ca/Si ratio generally ranges from 0.7 to 2.0, with a mean value of 1.75 for hydrated Portland cement (7). H.F.W. Taylor (5) identified two types of C-S-H: C-S-H (I), which forms for Ca/Si ratios less than 1.5 and whose structure is close to that of Tobermorite, and C-S-H (II), observed for Ca/Si ratios greater than 1.5, presenting a structure similar to that of Jennite, another natural lamellar mineral. A. Nonat et al. (8,9), therefore, suggested a categorization of three types of C-S-H systems: C-S-H (I) for Ca/Si ratios < 1, C-S-H (II) for 1 < Ca/Si < 1.5 and C-S-H (III) for Ca/Si > 1.5. Another study (10) reported that the Ca/Si ratio of C-S-H in hydrated Portland cement can reach higher values and can reach 3, although the majority of values are between 1.3 and 1.8.

Both calcium and silicon exhibit significant antifungal activity, although based on different mechanisms. Calcium hydroxide, released from materials such as CEM cement, dissociates into Ca^{2+} and OH^- ions, leading to an increase in the pH of the medium, which inhibits fungal growth, this effect is enhanced by the diffusion of active components present in the material (11). Moreover, calcium particularly in the form of nanoparticles, has demonstrated direct antifungal efficacy when used as a deacidification treatment (12). As for silicon, generally used in the form of sodium silicate, it exerts concentration-dependent fungal inhibition, as observed on the genera Penicillium, Fusarium, Alternaria and Trichothecium; this activity is thought to be linked to an increase in pH and physiological effects on fungal spores (13, 14).

Furthermore, silicon can also induce an antifungal response by stimulating the production of defense compounds (15). Furthermore, the recent studies have shown that the addition of nanomaterials such as ZnO and TiO_2 promotes the formation of C–S–H gel, while strengthening the adhesion between aggregates and the cement matrix (16). Furthermore, the Ca/Si ratio plays an essential role not only in the nucleation and quantity of C–S–H formed, but also in the internal structuring of this gel and its mechanical properties (17).

Microbial attacks, particularly from bacteria and fungi, degrade concrete through biofilm formation, leading to chemical damage, cracking, and reduced mechanical strength (18). Fungi, such as *Penicillium chrysogenum* and *Aspergillus versicolor*, are primary contributors to the bio-deterioration of both organic and inorganic materials. They produce organic acids, such as oxalic acid, which react with concrete to form insoluble calcium complexes, causing material degradation. These fungi are commonly found in water-damaged buildings, promoting concrete discoloration and increased porosity (10). Microorganisms in corroded concrete often include species such as *Thiobacillus* and *Acidithiobacillus* (19). Antimicrobial materials, including metals like Fe, Zn, Mn, Mo, Ni, and Ti, inhibit microbial growth by interacting with microbial cells in the acidic environments created by microorganisms. Zinc oxide (ZnO) is widely used in construction materials for its antimicrobial properties, comparable to commercial biocides (18). Studies have shown that nanoparticles of metals and metal oxides, such as silver, copper, titanium oxide, zinc oxide, and copper oxide, are effective in preventing microbial growth. These nanoparticles enhance the longevity of building materials and enable bioactive coatings for existing structures, including historical buildings. Their antimicrobial efficiency depends on their properties (size, shape, surface area, concentration) and the substrate's characteristics (porosity, absorbability, pH), as well as environmental factors like humidity, temperature, and material degradation (19). Biofilm formation on concrete leads to discoloration and tarnish, followed by chemical deterioration due to acidic metabolites excreted by bacteria, which lowers the pH, increases porosity, and reduces mechanical properties (19). Recent research indicates that ZnO nanoparticles are particularly effective, acting as semiconductors that degrade pollutants and inhibit microbial activity through the release of Zn^{2+} ions and reactive oxygen species (ROS) generation (20). ZnO is utilized in construction for its photocatalytic properties and ability to inhibit fungal growth, even in low-light conditions, by disrupting microbial membranes and enzymatic functions. Incorporating ZnO into cement has been shown to significantly reduce fungal growth, enhancing the material's durability (21, 22). TiO_2, widely used in orthopedic and dental implants, also demonstrates antimicrobial properties, primarily activated by UV light. It prevents microbial adhesion by producing ROS, which disrupt microbial cells (23). TiO_2-based paints applied to steel and concrete surfaces have effectively inhibited the growth of fungi such as *Aspergillus niger and Trichoderma viride* (24). Research indicates that antimicrobial agents in concrete affect its technical properties based on their chemical reactivity and the concrete's constituents (25). ZnO and TiO_2 enhance the concrete's strength and durability while providing antifungal properties, making them essential in sustainable construction practices (26). ZnO has been shown to inhibit fungal growth more efficiently than TiO_2, especially under high-nutrient conditions (27). The literature demonstrates the effectiveness of metal and metal oxide nanoparticles, such as ZnO and TiO_2, in inhibiting microbial growth, with their efficacy dependent on their physicochemical properties and the substrate material's characteristics. Environmental factors influencing microbial activity also play a crucial role in determining the durability and protection of construction materials (19).

The aim of this work is to evaluate the influence of ZnO and TiO_2 nanoparticles incorporation on the microstructure and composition of cement hydrates (C-S-H), in relation to their self-cleaning and antifungal properties in order to describe the types of C-S-H formed in the hydrates and to optimize the material formulation for sustainable and hygienic construction applications. A particular focus is placed on the correlation between the Ca/Si ratio and antifungal performance, a relationship that remains underexplored in the literature. Moreover, a new alternative method for the indirect determination of the Ca/Si ratio in C-S-H gel is proposed, combining data from X-ray diffraction (XRD), X-ray fluorescence (XRF), and thermogravimetric analysis (TG), offering a more accurate and complementary estimation approach.

2. MATERIALS AND METHODS

2.1. Materials

The chemical and mineralogical composition of the commercial cement CEM I 42.5 R, which was used for the preparation of cement pastes with ZnO and TiO_2 nanoparticles during a hydration period of 28 days, is presented in Table 1. The high percentages of CaO oxides and C_3S phase, compared to the other components, indicate that this cement is particularly rich in calcium.

Table 1. Chemical and mineral composition of CEM I 42.5 R (% by weight).

Chemical composition [%]									Mineral composition [%]			
SiO_2	Al_2O_3	Fe_2O_3	CaO	MgO	SO_3	K_2O	TiO_2	P_2O_5	C_3S	C_2S	C_3A	C_4AF
18.7	4.5	3.4	65.9	1.3	4.3	0.8	0.3	0.1	66.0	13.8	9.1	7.6

In this work, the used nanomaterials were zinc oxide (ZnO) and titanium dioxide (TiO_2). ZnO was produced by the Czech company Radka and was synthesized by the vaporization of metallic zinc followed by oxidation in air. It has a broader crystallite size of about 60 nm and significantly lower BET surface area of 10-15 m^2/g. The company Precheza from Czech Republic provided TiO_2 which is made of 99% pure anatase and containing some sulphates (0.7% by weight) implying the use of sulphate process in its production. It has a small crystallite size of 12 nm and high BET surface area of approximately 100 m^2/g. Scanning Electron Microscopy (SEM) analysis (Figure 1) revealed that ZnO nanoparticles have a variety of morphologies including nanotubes 200-400 nm in length with hexagonal cross sections (diameter 20-40 nm) and hexagonal nanoprisms with lateral dimensions of 150-450 nm (Figure 1(A)). On the other hand, TiO_2 nanoparticles form agglomerates with uniform spherical shapes and particle sizes between 20-30 nm (Figure 1(B)).

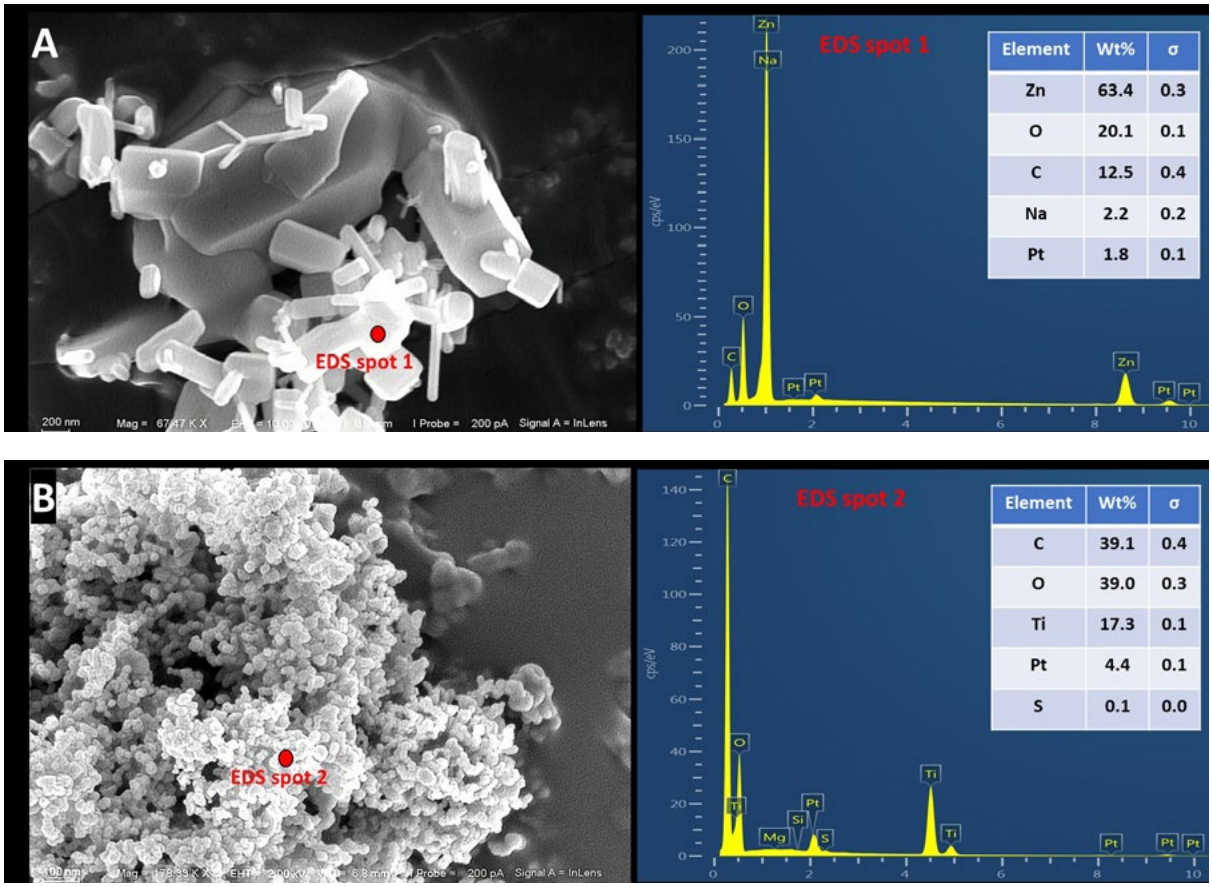

Figure 1. SEM images and EDS Spectra of (A) (67.4k x magnification) ZnO and (B) TiO_2 (178k x magnification).

Analysis of TiO_2 by energy-dispersive spectroscopy (EDS) showed the presence of mainly Ti and O. The notable carbon signal displayed stemmed from contamination of the sample holder used during the analysis.

2.2. Methods

- ZnO and TiO_2 oxides powder and cement were used to prepare hydrated samples. Nine series of cement pastes were formulated, designated as C, CT1, CT2, CT3, CZ0.3, CZ0.6, CZ1, CT1Z0.6, and CT2Z0.3, following the compositions detailed in Table 2. The cement pastes were hydrated using distilled water with a water cement (W/C) ratio of 0.4 and cast into prismatic moulds measuring 20×20×100 mm. After curing in water for 28 days, the samples were air-dried at room temperature (23 ± 1 °C) for 24 hours. The cured samples, incorporating various percentages of nanoparticles, were ground and analysed using different techniques, including X-ray diffraction (XRD), X-Ray Fluorescence (XRF), Differential Scanning Calorimetry (DSC), and Thermogravimetric (TG) analysis and antifungal activity, all performed after 28 days of hydration.

Table 2. Composition of cement paste formulations.

	C	CT1	CT2	CT3	CZ0.3	CZ0.6	CZ1	CT1Z0.6	CT2Z0.3
Cement (C) (%)	100	99	98	97	99.66	99.33	99	98.33	97.66
TiO_2 (T) (%)	0	1	2	3	0	0	0	1	2
ZnO (Z) (%)	0	0	0	0	0.34	0.67	1	0.67	0.34

- X-ray diffraction (XRD) analysis of cement pastes was performed using a PANalytical Aeris diffractometer with CoKα radiation operating at 40 kV and 7.5 mA. The measurements were performed in the Bragg-Brentano geometry with an angular range of 5 to 85° (2θ), a step size of 0.0217° and a scan time of approximately 1 h. The instrument is equipped with 0.04 rad Soller slits, a 13 mm mask, a 1/2° divergence slit on the incident beam side and a 9 mm anti-scattering slit on the diffracted beam side. The detector PIXcel1D-Medipix3 was employed with an active length of 5.542°. Approximately 2 g of powdered sample was analysed without background correction. Phase quantification was performed using the Rietveld refinement method with Profex software incorporating an internal standard of 20% ZnO to estimate the amorphous fraction (28).
- The chemical composition of the samples was analysed using X-ray fluorescence (XRF) using the Genius IF device, available at the Technopark in Kralupy, Czech Republic. This method is based on how X-rays from a metal target interact with the material being sampled. The resulting secondary X-ray emissions are characteristic of the elements present because their frequencies are correlated with the atomic numbers of the emitting atoms, which allows for precise elemental identification.
- The microstructural morphology of the nanoparticles was analysed with a Zeiss Merlin ultra-high-resolution field emission scanning electron microscope (FEG-SEM) equipped with a Schottky cathode. The Gemini II column of the instrument enables versatile scanning modes, allowing thus probe currents ranging from a few picoamperes (pA) for high-resolution imaging to 300 nanoamperes (nA) for analytical applications.
- The thermal behavior of the samples was investigated using simultaneous Differential Scanning Calorimetry and Thermogravimetry DSC-TG (SetaramLabsys Evo). Approximately 50 mg of powdered material was placed in an alumina crucible with a lid and heated from 25 to 1000 °C at 10 °C/min under a 40 mL/min argon purge. The content of portlandite was determined according to the procedure outlined by Dweck et al. (29). Portlandite CH content was quantified by thermogravimetric analysis TG, by measuring the mass loss associated with its dehydration on the derivative thermogravimetric DTG curve (30).
- The Ca/Si ratios of the C-S-H phases in the different cement pastes were calculated to estimate the composition of the C-S-H phases formed during hydration. The proportions of unreacted C_3S and C_2S were determined by phase quantification using the Rietveld refinement method on

XRD data and then were used as a basis for calculating the amounts of CaO and SiO_2 released during their hydration. A simplified stoichiometric ratio was applied: 1.5 CaO per 0.5 SiO_2 for C_3S and 1 CaO per 0.5 SiO_2 for C_2S. A correction was subsequently introduced to account for the consumption of CaO due to the formation of portlandite CH as quantified by XRD and TG. The final Ca/Si ratio was calculated by dividing the corrected amount of CaO by the total SiO_2. While acknowledging that the true stoichiometry of C-S-H can change, this simplified method offers an estimate of its average composition. This method, inspired by several works in the literature (31–33), was adapted by considering the stoichiometry of silicate hydration reactions.

- Ca/Si ratios were also calculated using an alternative method based on XRF data to provide a global estimate of their evolution. This technique allows to determine the mass percentages of CaO and SiO_2 oxides present in each sample and to use them in the calculations. The Ca/Si ratio is determined by directly dividing the percentage of CaO by that of SiO_2. However, this approach has significant limitations because X-ray fluorescence analysis does not differentiate the distribution of oxides between the different phases, in particular between CH and C-S-H. Consequently, the Ca/Si ratio from XRF represents a global ratio and does not accurately reflect the stoichiometry of the C-S-H phases formed and which is influenced by hydration reactions and the presence of other phases. It is therefore a complementary and approximate estimate useful for observing general trends, but which does not allow a precise quantitative analysis of the C-S-H composition.

2.3. Anti-fungal activity evaluation

– Testing procedure

In the context of evaluating antifungal activity, cement samples were carefully immersed in distilled water for 24 hours. After this period, the pH of the water provided an accurate reading of the solution's acidity. The resulting aqueous leachate was then adjusted to a pH range between 6.5 and 7.5, an optimal range to promote fungal growth. This leachate was used to prepare 10% Czapek-Dox Agar, which was evenly distributed into Petri dishes. Once the medium was prepared, it was inoculated with three fungal species known for their pathogenic potential: *Penicillium brevicompactum, Trichoderma reesei*, and *Aspergillus niger*. A control was also set up by inoculating a Czapek-Dox medium prepared with distilled water and enriched with nutrients at respective concentrations of 100 and 10%. This control was inoculated with the same fungi to compare the results with the concrete samples. Finally, to ensure stable temperature conditions conducive to fungal growth, all Petri dishes were placed in a biological incubator set to 26°C.

– Measurement of antifungal effect

After introducing the liquid medium into the flask, the aforementioned constant concentration of spores became colloidal. A sample disc incorporating antifungal agents was placed in the center of the flask, previously sprayed with the spores using the same procedure. The flask was then sealed and incubated to prevent contamination by other fungi. The detailed and sequential measurement procedure is illustrated in the corresponding figure. To estimate the antifungal inhibition zone, the criteria presented in Figure 2 and Equation [1] consist of calculating the length obtained by subtracting the radius of the sample disc from the distance between the center of the sample and the outer edge of the inhibition zone. This allows quantification of the antifungal effect of the cement mortar containing the active agents. The precise size of the inhibition zone is calculated according to Equation [1]:

$$I = (I_1 + I_2) / 2 \qquad [1]$$

Where:

– Major axis: $I_1 = D_1 - R_1$
– Minor axis: $I_2 = D_2 - R_2$

With:

- I: represents the average width of the inhibition zone (in mm).
- D: is the distance from the center of the mortar disk to the fungal growth limit (in mm).
- R: is the radius of the antifungal samples disk (in mm).

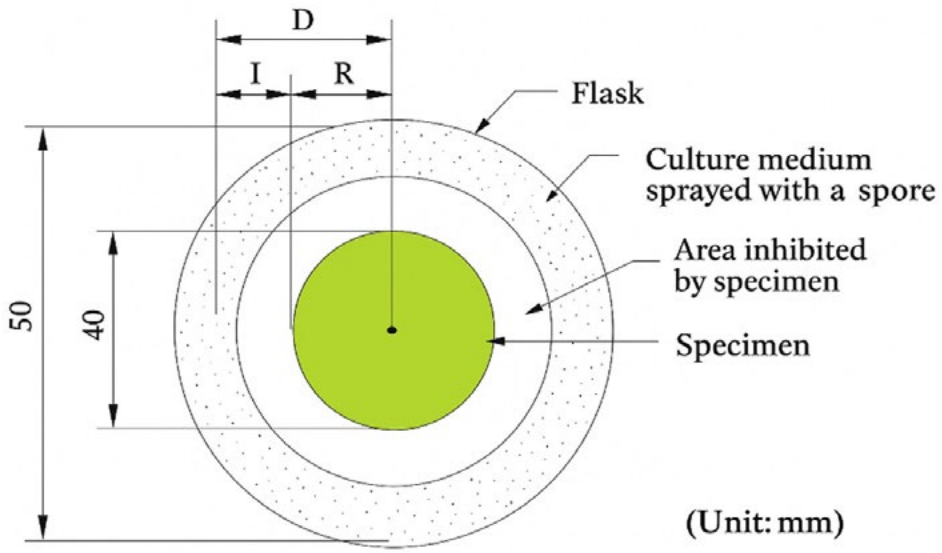

Figure 2. Measurement of antifungal zone.

3. RESULTS AND DISCUSSION

3.1. Ca/Si ratios calculated from XRD data

Table 3 presents the phase quantification results by XRD and the corresponding Ca/Si ratios. This part examines the influence of ZnO and TiO_2 nanoparticle additions on the Ca/Si ratio of the C-S-H phases formed after 28 days of hydration, with the aim of establishing a link with the mechanical performances studied in our previous work on concretes of identical formulations (34, 35). The Ca/Si ratio is an important indicator of the structure and properties of C-S-H and the main contributor to the strength of concrete (36). The Ca/Si ratio of the reference paste C is 2.67 representing the basic composition of C-S-H in the absence of additions.

Table 3. Phase quantification and Ca/Si ratios (XRD).

	C	CT1	CT2	CT3	CZ0.3	CZ0.6	CZ1	CT2Z0.3	CT1Z0.6
Unreacted C_3S (%)	15.33	19.28	15.40	36.80	45.67	51.4	54.4	18.60	23.01
Unreacted C_2S (%)	11.10	13.36	12.90	12.27	13.21	7.67	10.27	9.31	9.54
Portlandite (%)	9.82	6.85	8.24	10.29	2.02	0.53	0.65	3.93	2.33
Ca/Si	2.67	2.77	2.74	2.44	2.83	2.67	2.7	2.80	2.83

The samples containing ZnO showed an increase in the amounts of unreacted C_3S and C_2S and a decrease in portlandite content. As is well established, zinc retards cement hydration by forming, at the early stages, a layer of crystalline calcium zincate ($Zn_2Ca(OH)_6 \cdot H_2O$) or amorphous zinc hydroxide ($Zn(OH)_2$) surrounding the anhydrous grains, which directly hinders the formation of C-S-H (37, 38). The influence on the Ca/Si ratio is nuanced; a slight increase is observed at a low dosage (CZ0.3: 2.83), while at higher dosages (CZ0.6: 2.67 and CZ1: 2.70), the values are similar to, or even slightly higher than, that of the reference. TiO_2 also influenced the Ca/Si ratio with a slight increase observed at low dosages (CT1: 2.77 and CT2: 2.74), followed by a more pronounced decrease at 3% (CT3: 2.44). The Ca/Si ratios of the samples CT2Z0.3 (2.80) and CT1Z0.6 (2.83) are between the values observed for the individual additions.

Mechanical strength tests on the corresponding concretes with the same formulation (35) revealed contrasting effects of the additions on performance. The addition of ZnO nanoparticles reduced mechanical strength, which can be explained by a slowdown in the hydration of silicates and a lower quantity of C-S-H formed, even though the Ca/Si ratios did not change significantly. In other words, it was primarily the quantity of C-S-H, rather than its composition, that influenced the strength. As for TiO_2, an increase in strength was observed at 1%, followed by a decrease at 2% and 3%, suggesting a complex effect on the microstructure. The initial increase might compensate for the slight rise in the Ca/Si ratio, whereas the subsequent decrease could be attributed to other factors, such as the formation of secondary phases (39), where the reduction in the Ca/Si ratio at 3% might be a contributing factor. Finally, the combined additions (CT2Z0.3 and CT1Z0.6) showed improved strength compared to individual additions of ZnO and, in the case of CT1Z0.6, compared to CT1, suggesting a synergistic effect on the microstructure (40), although variations in the Ca/Si ratio remained moderate. A. U. Adebanjo et al. (41) reported that the addition of TiO_2 and ZnO nanoparticles to the concrete mixture had a notable influence on the composition and the Ca/Si ratio of the hydration products. This result corroborates the findings of this study.

The obtained values of the Ca/Si ratios of C-S-H and even those after correction for portlandite are generally higher than the commonly accepted range of 1.5 to 2 (42). This observation can be attributed to several factors. First, the cement used (CEM I 42.5 R) is intrinsically rich in CaO. This basic composition directly influences the stoichiometry of the hydrated phases, in particular that of C-S-H (43). The high proportion of C_3S (66%) in the clinker may also contribute to this calcium richness. Second, the calculation model used is based on simplifications, even if it is useful to compare estimates between samples. The actual stoichiometry of C-S-H is variable and may deviate from the simplified formula $C_3S_2H_8$. Furthermore, the calculation does not take into account other potentially present hydrated phases (e.g., hydrated aluminates), which could also influence the CaO balance (31). Our results are consistent with those of E. Lachowski et al. (10), who reported that the Ca/Si ratios observed in C-S-H can reach high values, ranging from 0.9 to just over 3.

3.2. Thermal analysis and Ca/Si ratios refined using TG data

The DTG curves of the hydrated cement pastes after 28 days are shown in Figure 3. These curves allow to identify the main stages of thermal decomposition of the hydrated phases by showing the mass loss rate as a function of temperature. Typically, three main peaks are observed in the DTG curves of hydrated cement pastes: peak between 100 and 200 °C corresponding to the dehydration of C-S-H and ettringite, as well as the evaporation of physically adsorbed water; peak between 400 and 550 °C corresponding to the dehydroxylation of portlandite ($Ca(OH)_2$); and peak between 600 and 900 °C corresponding to the decarbonation of calcium carbonate ($CaCO_3$) formed by carbonation (44). The intensity of the peaks between 400 and 550 °C is proportional to the amount of portlandite in the sample. This agrees well with the values in Table 4, where the phase quantifications of portlandite were indicated for both TG and XRD analyses. For example, cement samples CZ0.6, CZ1 and CT1Z0.6 with the lowest amounts of portlandite also show the most reduced peaks in this temperature range on the DTV curves. Conversely, samples C, CT2 and CT3 with the highest amounts of portlandite show the most intense peaks on the DTV curves. The peaks associated with the dehydration of C-S-H and ettringite in samples CZ0.3, CZ0.6 and CZ1 are less intense, indicating a lower amount of hydrated C-S-H phases. This phenomenon is consistent with the results of P. Siler et al. (45), which showed that zinc nanoparticles induce a hydration delay. Cement pastes containing TiO_2 and the reference cement C showed significantly higher intensity peaks, which agrees with the values in Tables 3 and 4, indicating a greater consumption of silicate phases and a significant formation of portlandite in these samples. These observations suggest that the presence of TiO_2 promotes the hydration of silicates. This is consistent with several studies that have shown that titanium oxide can have a beneficial effect on cement reactivity and, consequently, on mechanical strength (34,35,46–51). Between 600 and 900 °C, zone associated with the decarbonation of $CaCO_3$, the intensity of the peaks for the zinc samples increases, indicating the formation of a greater amount of $CaCO_3$. This may be related to a greater carbonation.

Figure 4 presents the quantified contents of the main hydration products of Portland cement, identified by thermogravimetric analysis (TGA/DTG), expressed on an ignited mass basis after 28 days of hydration. This representation enables a direct comparison of portlandite, C–S–H, and $CaCO_3$ contents among the different samples. The figure is complemented by a quantitative analysis derived from the corresponding weight losses, providing clearer insights into the hydration process. The results reveal that portlandite content decreases significantly in Zn-doped samples, while TiO_2 additions lead to higher C–S–H formation. These observations are in good agreement with the XRD results shown in Table 3, confirming that Zn strongly inhibits hydration, whereas TiO_2 promotes it.

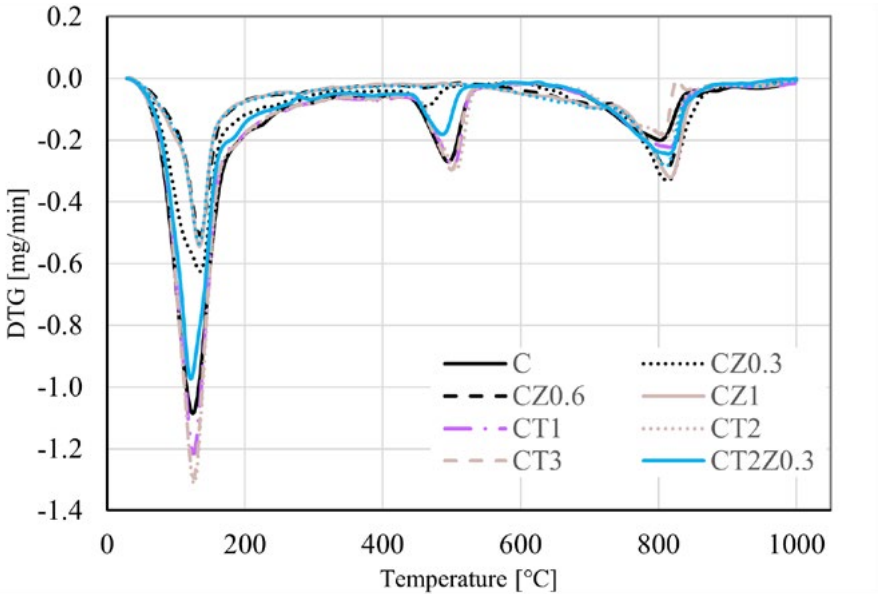

Figure 3. DTG curves of cement pastes after 28 days.

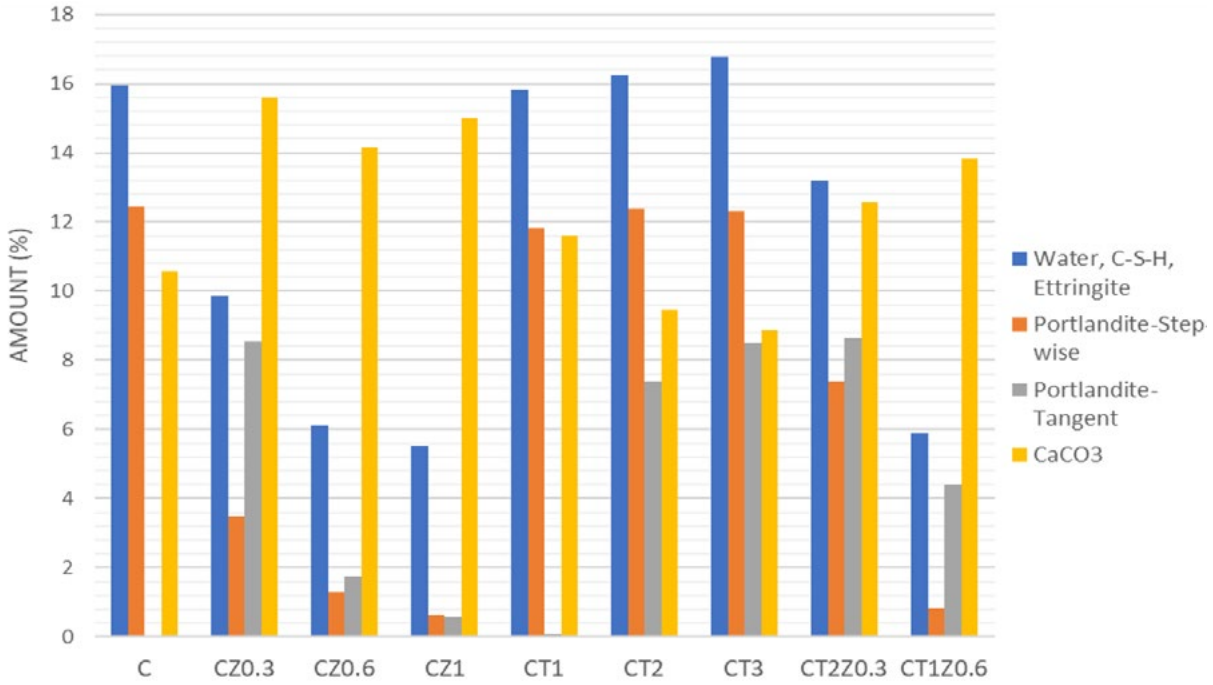

Figure 4. Quantified amounts (%) of main hydration products in cement pastes after 28 days of curing.

Table 4. Phase quantification and Ca/Si ratios (XRD, TG).

	C	CT1	CT2	CT3	CZ0.3	CZ0.6	CZ1	CT2Z0.3	CT1Z0.6
Unreacted C_3S (%)	15.33	19.28	15.40	36.80	45.67	51.40	54.40	18.60	23.01
Unreacted C_2S (%)	11.10	13.36	12.90	12.27	13.21	7.67	10.27	9.31	9.54
Portlandite XRD (%)	9.82	6.85	8.24	10.29	2.02	0.53	0.65	3.93	2.33
Portlandite TG (%)	10.48	9.62	10.44	10.48	2.62	0.94	0.37	5.90	0.51
Ca/Si XRD	2.67	2.77	2.74	2.44	2.83	2.67	2.70	2.80	2.83
Ca/Si TG	2.65	2.68	2.67	2.43	2.78	2.64	2.73	2.74	2.89

Table 4 presents a comparison of the Ca/Si ratios of C-S-H calculated from the XRD data, with those recalculated using the portlandite values derived from the TG analysis. The quantified portlandite content corresponds to the average value obtained from both the step-wise and tangent methods. The aim is to evaluate the impact of using more accurate experimental data of the portlandite phase on the estimation of the Ca/Si ratio. Overall, the Ca/Si ratios calculated from XRD data and those corrected using TG data are very similar, indicating good consistency between the two methods of portlandite quantification. As observed by F. Georget et al. (52), our results also show relative agreement between portlandite measurements obtained by TG and XRD. The differences, although minor, demonstrate the impact of the accuracy of the portlandite calculation on the Ca/Si ratio. The interpretation of the data previously observed in Table 3 regarding the influence of the additions on the Ca/Si ratio remains largely consistent, making it an additional validity. The use of TG data for portlandite correction provides a minor but significant improvement in the estimation of the Ca/Si ratio. Both methods yield consistent results; however, the use of TG data, being more direct, is preferable for greater accuracy.

3.3. Ca/Si ratios from X-Ray fluorescence (XRF) analysis

Figure 5 showed the chemical composition of cement pastes obtained by XRF analysis after 28 days of hydration. The results of this analysis provided a detailed overview of the elemental oxide composition of the cement pastes. A predominance of CaO and SiO_2 was found with variations attributed to the different additions. The incorporation of TiO_2 led to a slight reduction in the CaO content and an increase in SiO_2 oxides, while the addition of ZnO nanoparticles led to a significant increase in the CaO and ZnO contents. When TiO_2 and ZnO nanoparticles were combined, their effects were found to be intermediate. Since XRF analysis provides overall information, these variations reflect the global compositional changes without specifically indicating the stoichiometry of the C-S-H phases.

Table 5 presents the CaO and SiO_2 oxide composition and the corresponding Ca/Si ratios of the C-S-H phases in the cement pastes after 28 days of hydration, as determined by XRF analysis. The addition of ZnO resulted in a significant increase in the Ca/Si ratio compared to the reference cement C whose ratio is 3.51. The higher the ZnO proportion (from 0.3 to 1%), the higher the Ca/Si ratio (3.79, 4.12 and 4.15 respectively). The addition of TiO_2 showed a more complex influence. A slight increase in the Ca/Si ratio was observed for CT1 (3.55) compared to the reference sample C, then a decrease for CT2 (3.32) and a further increase for CT3 (3.44). Samples with combined additions of TiO_2 and ZnO showed Ca/Si ratios intermediate between those observed for the individual additions. CT1Z0.6 (3.8) lies between CT1 (3.55) and CZ0.6 (4.12), while CT2Z0.3 (3.61) lies between CT2 (3.32) and CZ0.3 (3.79). This probably indicates an interaction between the effects of TiO_2 and ZnO on the composition of C-S-H (53). As shown by A.U. Adebanjo et al. (41), nanoparticle addition in High Performance Concrete significantly affects morphology and elemental composition, leading to reduced C-S-H and lower Ca/Si ratios, indicating structural and compositional changes. The combined addition appears to attenuate the increase in Ca/Si ratio induced by ZnO alone. The interaction between TiO_2 and ZnO in the combined additions suggests that these two oxides influence hydration in an interdependent manner, modifying the composition of the hydrates formed (54).

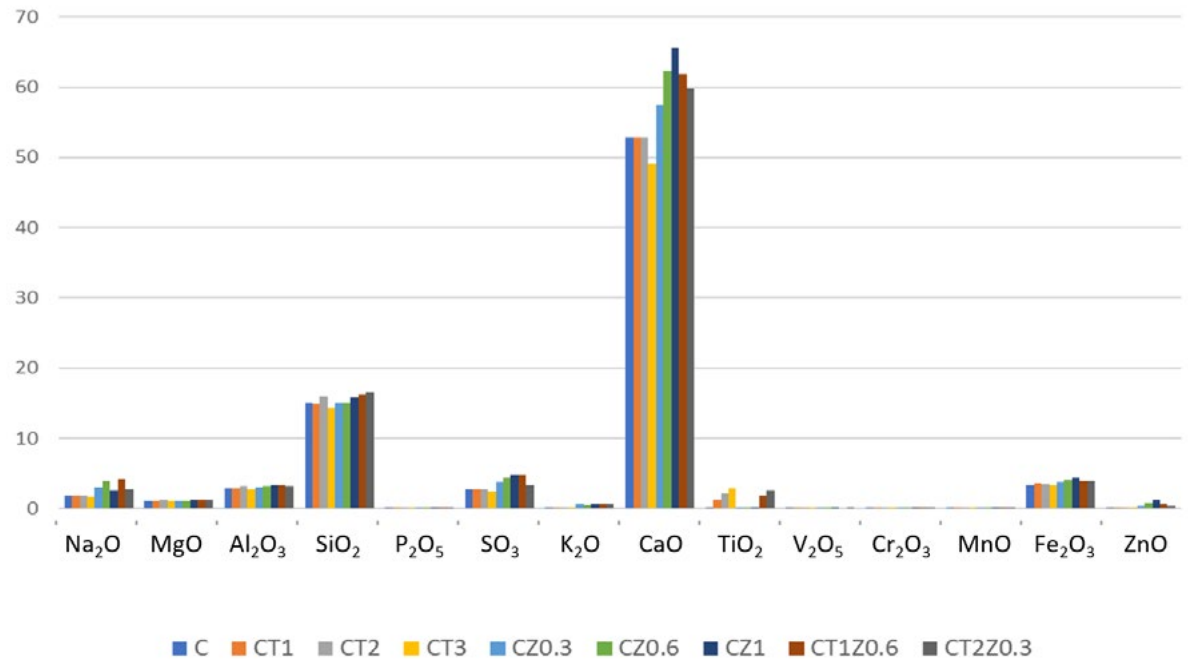

Figure 5. XRF analysis of cement paste oxide composition.

Table 5. Quantification of phases and Ca/Si ratios (XRF).

	C	CT1	CT2	CT3	CZ0.3	CZ0.6	CZ1	CT1Z0.6	CT2Z0.3
CaO	52.86	52.86	52.74	49.08	57.4	62.27	65.61	61.92	59.74
SiO2	15.07	14.9	15.89	14.35	15.09	15.12	15.8	16.3	16.57
Ca/Si	3.51	3.55	3.32	3.44	3.79	4.12	4.15	3.8	3.61

3.4. Evolution of Ca/Si ratios obtained by different techniques (XRD, TG, XRF)

Figure 6 presented the comparative graph of the Ca/Si ratios by the three analytical techniques XRD, TG and XRF. The values obtained from the XRF analysis indicate significant deviations from the values obtained by the other two techniques. These deviations highlight the limitations of the direct use of XRF data for the precise calculation of the Ca/Si ratio in C-S-H. XRF gives a global elemental analysis of the sample, providing the proportions of the different oxides present. However, there is no consideration of how these oxides are distributed between the different hydrated phases, in particular portlandite, and C-S-H which have a variable stoichiometry (55). Thus, the direct calculation of the Ca/Si ratio based on XRF data without any correction significantly overestimates the amount of CaO contained in the C-S-H phase, leading to higher values, as observed in the graph. On the other hand, the combined XRD and TG approach allowed a more accurate estimation. XRD data provide indirect information on the amounts of reacted C_3S and C_2S, allowing to calculate the amounts of CaO and SiO_2 consumed during the formation of C-S-H. In addition, TG data allowed to quantify the portlandite formed, which is crucial to correct the CaO balance and obtain a Ca/Si ratio more characteristic of the C-S-H formula. Thus, the values obtained by this combined approach are considerably lower and closer to the values typically reported in the literature for hydrated C-S-H (7, 36, 43, 56, 57).

To conclude, the Ca/Si ratios found in this work by the three techniques are greater than 2 in all samples. They are in the high range of values reported in the literature for hydrated C-S-H of Portland cement, which can reach 3 (10). These values suggest the formation of C-S-H type II according to the classification of H.F.W. Taylor (5), whose structure is similar to that of Jennite, or type III according to Nonat et al. (8, 9), characterized by a Ca/Si ratio greater than 1.5. Our results therefore indicate a predominance of C-S-H with a less ordered structure, typical of high Ca/Si ratios.

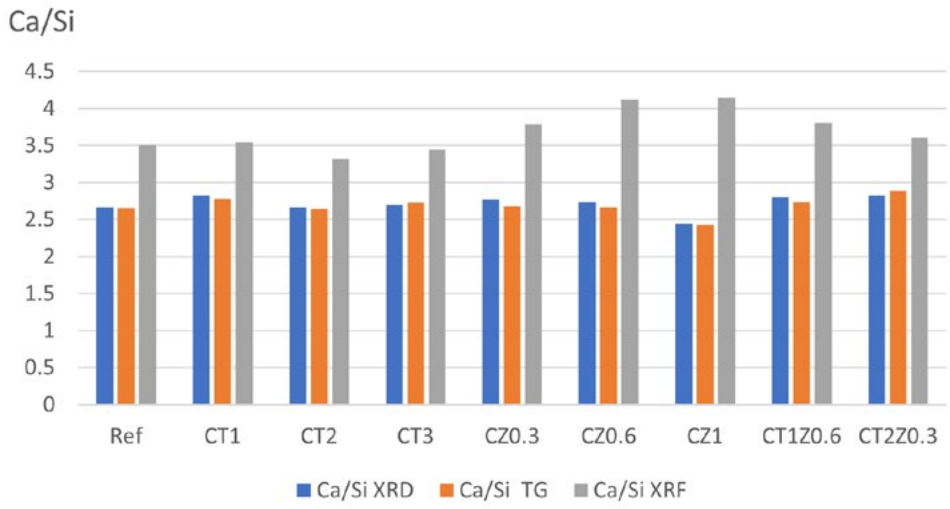

Figure 6. Ca/Si ratios determined by XRD, TG and XRF.

3.5. Antifungal activity of cement pastes

Figure 7 showed the digital photos of fungal cultures containing the samples. The growth grades based on visual observations of three fungal strains in each case. The test results indicated that the addition of TiO_2 and ZnO in concrete formulations significantly influences the growth of fungi *Penicillium brevicompactum, Trichoderma reesei*, and *Aspergillus niger* (Table 6 and Figure 8). Samples containing only cement (C) showed moderate fungal growth, suggesting that cement alone has a limited inhibitory effect. The addition of TiO_2 (CT1 to CT3) leads to a progressive decrease in fungal growth, with notable inhibition at higher concentrations (CT3 with 3% TiO_2), which can be attributed to the photocatalytic and antimicrobial properties of TiO_2 (58). This aligns with previous findings where P25 TiO_2, when integrated into cementitious matrices, demonstrated significant antifungal activity against Aspergillus species under UV exposure (59). Although the TiO_2 material used in our study differs from P25 in terms of phase composition and surface characteristics, the comparable level of inhibition supports the conclusion that the photocatalytic properties of TiO_2 play a major role in controlling fungal proliferation in cement-based systems.

Similarly, samples with ZnO (CZ0.3 to CZ1) exhibit increasing fungal growth reduction as the ZnO percentage increases, reflecting the well-known antifungal properties of this oxide (21). Samples combining TiO_2 and ZnO (CT1Z0.6 and CT2Z0.33) display even more pronounced inhibition, suggesting a synergistic effect between these two additives. The pH of the leachates, generally alkaline and ranging from 10.88 to 11.50, might also play a role in this inhibition by creating a less favourable environment for fungal growth. Overall, these results highlight the enhanced efficacy of formulations containing combinations of TiO_2 and ZnO in limiting fungal growth, offering promising prospects for applications requiring increased biological resistance in concrete materials. Generally, the incorporation of ZnO and TiO_2 in cement system was found to have a significant effect on fungal growth inhibition at all applied strains. The results of the anti-fungal activity test reveal the promising potential of ZnO oxide and TiO_2 oxide in controlling fungal growth, particularly on construction materials such as concrete, where fungi can cause significant damage (19). Fungi, being ubiquitous in the environment, require specific conditions such as water availability, pH, and nutrient sources for colonization (60). ZnO oxide has demonstrated effective antifungal activity, notably against molds like *Aspergillus niger* and *Penicillium brevicompactum* (61). Furthermore, research has shown that incorporating ZnO into cement enhances its antibacterial and antifungal properties (62). ZnO's antibacterial effectiveness is attributed to its polarized surfaces, caused by zinc (Zn^{2+}) or oxygen (O_2-) ions, which generate free radicals and reactive oxygen species (ROS), inducing oxidative stress in microbial cells (62). These free radicals further contribute to its antimicrobial properties (63). Similarly, A study has demonstrated that $Ca(OH)_2$-ZnO and $Ca(OH)_2$-TiO_2 materials exhibit antifungal activity (64). Another study demonstrated that the

incorporation of ZnO in cement composites exhibited antifungal activity, showing almost no growth at a 15% ZnO concentration (62). On the other hand, TiO_2 oxide has been shown to reduce fungal colonies through its photocatalytic properties, with the incorporation of up to 5% by weight leading to enhanced resistance against microbial growth and confirming its self-cleaning potential in construction materials (65). Both oxides act similarly, offering a dual approach to preventing the discoloration of biofilms caused by fungi and algae on building façades (66). In addition, shifts in pH, such as those caused by fungal infections, can inhibit fungal growth by creating stress on their cells, limiting nutrient acquisition and reducing the availability of essential elements like iron and copper, further supporting the antifungal effects of these oxides (67). Compared to the results observed previously, this study found that incorporating low percentages of the combination of TiO_2 and ZnO into the samples CT1Z0.6 and CT2Z0.3 resulted in significant antifungal activity. The incorporation of TiO_2 and ZnO at these concentrations demonstrated a notable ability to inhibit fungal growth, demonstrating their potential as effective additives in cement. These findings suggest that even small amounts of these oxides can effectively enhance the antifungal properties of the samples (Table 6). The Influence of the Ca/Si Ratio on the percentage of inhibition, presented in Figure 8, shows that the inhibition zone and the percentage of inhibition generally increase when the Ca/Si ratio is adjusted to values around 2.5–2.9, and that some sample combinations (CT1Z0.6 and CT2Z0.3) provide high antifungal efficacy. This effect can be partly explained by the influence of zinc and titanium ions, which promote C–S–H gel nucleation and growth, thereby enhancing the structure and active surface of the material. The addition of ZnO and TiO_2 can act as heterogeneous nucleation sites, accelerating the formation of C–S–H (16) and strengthening its interaction with antifungal agents (11, 15). These results indicate that optimizing the Ca/Si ratio can significantly improve the antifungal properties of the samples.

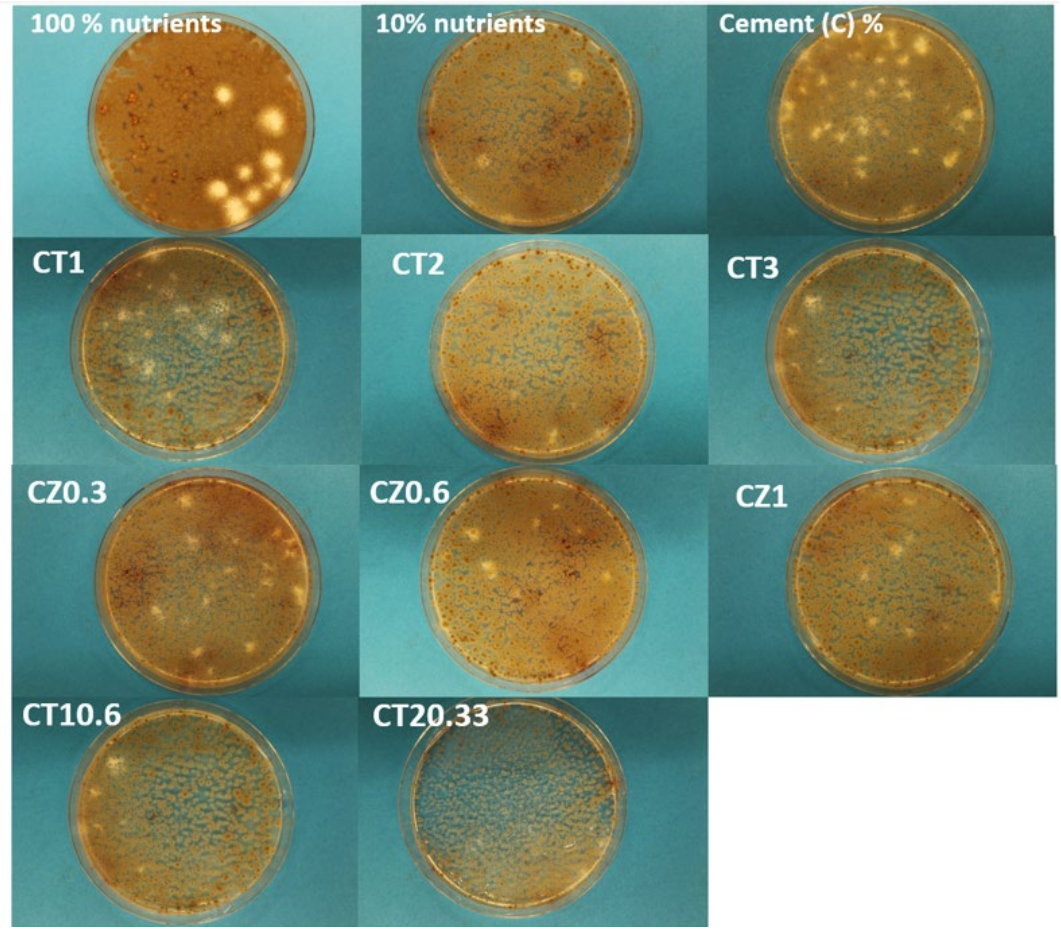

Figure 7. Digital photos of different types of fungal cultures affecting Portland cement (C), with and without ZnO and TiO_2.

Table 6. Fungal growth inhibition parameters and corresponding Ca/Si Ratios and pH values for different samples.

Sample	Diameter (mm)	Inhibition zone (mm)	Inhibition (%)	Ca/Si ratio	pH
100% Nutrients (control)	54	0	0.00	–	-
C	49	5	9.26	2.65	10.88
CT1	34	20	37.04	2.68	11.20
CT2	23	31	57.41	2.67	11.21
CT3	22	32	59.26	2.43	11.50
CZ0.3	30	24	44.44	2.78	11.10
CZ0.6	27	27	50.00	2.64	11.14
CZ1	24	30	55.56	2.73	11.45
CT1Z0.6	20	34	62.96	2.74	11.21
CT2Z0.3	21	33	61.11	2.89	11.34

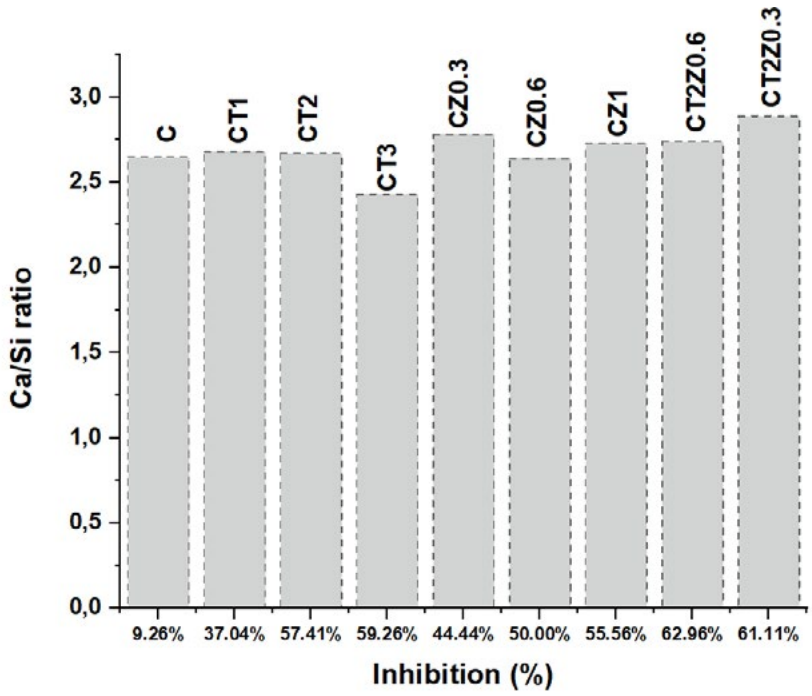

Figure 8. Influence of the Ca/Si Ratio on the percentage of inhibition.

4. CONCLUSIONS

This study shows that TiO_2 and ZnO nanoparticles can tailor the hydration behavior, microstructure, and antifungal activity of cementitious systems. Based on the results:

- The incorporation of TiO_2 increases apparent reactivity and promotes the formation of hydration products; XRD, XRF, and TG provide consistent trends indicating improved reactivity.
- The Ca/Si ratios of the C-S-H phases obtained by XRD and TG are generally concordant and lower than the values obtained by XRF. This difference is due to the indirect data on the quantities of reacted C_3S and C_2S that allowed to calculate the quantities of CaO and SiO_2 consumed during the formation of C-S-H, thus emphasizing the importance of correcting the XRF data to take into account the presence of portlandite. The Ca/Si values obtained by XRD and TG were greater than 2 for all samples, thus suggesting the formation of C-S-H of type II according to Taylor or

type III according to Nonat, with a less ordered structure.

- Adding ZnO and TiO_2, alone or in combination, confers significant antifungal activity to cement paste against Penicillium brevicompactum, Trichoderma reesei, and Aspergillus niger. TiO_2 is generally more effective than ZnO, and low-dose combinations of both oxides are particularly effective in inhibiting microbial growth.
- The adjustment of the Ca/Si ratio improves the antifungal properties of the material.

These findings support optimizing nanoparticle dosage and combinations to develop multifunctional, durable, and hygienic cement-based materials.

Supplementary information ↑

Funding sources

The authors of this article declare that they have no financial, professional or personal conflicts of interest that could have inappropriately influenced this work.

Supplementary material

Not applicable.

Data availability

Not applicable.

Acknowledgements

The authors express their gratitude to ''Mobility Faculty of Civil Engineering'', Projects "Mobility Czech Technical University in Prague'' Program for the financial support given in order to support this original research.

Authorship contribution statement

Fouad Amor: Conceptualization, Methodology, Research, Formal analysis, Validation, Write-up – original draft.

Hind Agourrame: Write-up – review & editing.

Zuzana Racova: Resources, Visualization.

Nacer Khachani: Write-up – review & editing.

Petr Hajek: Supervision, Fund raising.

Competing interests

The authors declare that they have no known financial conflicts of interest or personal relationships that could have influenced the work reported in this article.

Statement on the use of Artificial Intelligence

Not applicable.

REFERENCES

1. Qi C, Manzano H, Spagnoli D, Chen Q, Fourie A. 2021. Initial hydration process of calcium silicates in Portland cement: A comprehensive comparison from molecular dynamics simulations. Cem. Concr. Res. 149:106576. https://doi.org/10.1016/j.cemconres.2021.106576

2. Tang S, Wang Y, Geng Z, et al. 2021. Structure, fractality, mechanics and durability of calcium silicate hydrates. Fract. Fractional 5(2):47. https://doi.org/10.3390/fractalfract5020047

3. Grutzeck M, Benesi A, Fanning B. 1989. Silicon-29 magic angle spinning nuclear magnetic resonance study of calcium silicate hydrates. J. Am. Ceram. Soc. 72(4):665-668. https://doi.org/10.1111/j.1151-2916.1989.tb06192.x

4. Klur I, Pollet B, Virlet J, Nonat A. 1998. C-S-H structure evolution with calcium content by multinuclear NMR. In: Nuclear Magnetic Resonance Spectroscopy of Cement-Based Materials. p. 119-141. https://doi.org/10.1007/978-3-642-80432-8_8

5. Taylor HFW. 1986. Proposed structure for calcium silicate hydrate gel. J. Am. Ceram. Soc. 69(6):464-467. https://doi.org/10.1111/j.1151-2916.1986.tb07446.x

6. Taylor HFW. 1950. Hydrated calcium silicates. Part I. Compound formation at ordinary temperatures. J. Chem. Soc. 0:3682. https://doi.org/10.1039/jr9500003682

7. Richardson IG. 1999. Nature of C-S-H in hardened cements. Cem. Concr. Res. 29(8):1131-1147. https://doi.org/10.1016/s0008-8846(99)00168-4

8. Nonat A. 1994. Interactions between chemical evolution (hydration) and physical evolution (setting) in the case of tricalcium silicate. Mater. Struct. 27(4):187-195. https://doi.org/10.1007/BF02473032

9. Nonat A, Lecoq X. 1998. The structure, stoichiometry and properties of C-S-H prepared by C_3S hydration under controlled condition. In: Nuclear Magnetic Resonance Spectroscopy of Cement-Based Materials. p. 197-207. https://doi.org/10.1007/978-3-642-80432-8_14

10. Lachowski E, Diamond S. 1983. Investigation of the composition and morphology of individual particles of Portland cement paste: 1. C-S-H gel and calcium hydroxide particles. Cem. Concr. Res. 13(2): 177-185. https://doi.org/10.1016/0008-8846(83)90100-X

11. Kangarlou A, Sofiabadi S, Yadegari Z, Asgary S. 2009. Antifungal effect of calcium enriched mixture cement against Candida albicans. Iran Endod. J. 4(3):101-105. https://pubmed.ncbi.nlm.nih.gov/24003330/

12. Sequeira SO, Laia CAT, Phillips AJL, Cabrita EJ, Macedo MF. 2017. Clotrimazole and calcium hydroxide nanoparticles: A low toxicity antifungal alternative for paper conservation. J. Cult. Herit. 24:45-52. https://doi.org/10.1016/j.culher.2016.12.004

13. Nabil M, Elnouby M, Al-Askar AA, Kowalczewski PŁ, Abdelkhalek A, Behiry SI. 2024. Porous silicon nanostructures: Synthesis, characterization, and their antifungal activity. Open Chem. 22(1). https://doi.org/10.1515/chem-2023-0169

14. Rémus-Borel W, Menzies JG, Bélanger RR. 2005. Silicon induces antifungal compounds in powdery mildew-infected wheat. Physiol. Mol. Plant Pathol. 66(3):108-115. https://doi.org/10.1016/j.pmpp.2005.05.006

15. Moreira LFN, Peña-Bengoa F, Niklander SE, da Silveira Bueno CE, de Martin AS, Rocha DGP. 2024. Comparative in vitro analysis of the antifungal activity of different calcium silicate-based endodontic sealers. Braz. J. Oral Sci. 23:e243355. https://doi.org/10.20396/bjos.v23i00.8673355

16. Al-saffar FY, Wong LS, Paul SC. 2023. An elucidative review of the nanomaterial effect on the durability and calcium-silicate-hydrate (C-S-H) gel development of concrete. Gels 9(8):613. https://doi.org/10.3390/gels9080613

17. Kunther W, Ferreiro S, Skibsted J. 2017. Influence of the Ca/Si ratio on the compressive strength of cementitious calcium–silicate–hydrate binders. J. Mater. Chem. A Mater. 5(33):17401-17412. https://doi.org/10.1039/C7TA06104H

18. Mohsen A, Ramadan M, Gharieb M, Yahya A, Soltan AM, Hazem MM. 2022. Rheological behaviour, mechanical performance, and anti-fungal activity of OPC-granite waste composite modified with zinc oxide dust. J. Clean Prod. 341:130877. https://doi.org/10.1016/j.jclepro.2022.130877

19. Ślosarczyk A, Klapiszewska I, Skowrońska D, Janczarek M, Jesionowski T, Klapiszewski Ł. 2023. A comprehensive review of building materials modified with metal and metal oxide nanoparticles against microbial multiplication and growth. Chem. Eng. J. 466:143276. https://doi.org/10.1016/j.cej.2023.143276

20. Mohsen A, Abdel-Gawwad HA, Ramadan M. 2020. Performance, radiation shielding, and anti-fungal activity of alkali-activated slag individually modified with zinc oxide and zinc ferrite nanoparticles. Constr. Build. Mater. 257:119584. https://doi.org/10.1016/j.conbuildmat.2020.119584

21. Aldosari MA, Darwish SS, Adam MA, Elmarzugi NA, Ahmed SM. 2019. Using ZnO nanoparticles in fungal inhibition and self-protection of exposed marble columns in historic sites. Archaeol. Anthropol. Sci. 11:3407-3422. https://doi.org/10.1007/s12520-018-0762-z

22. Joni IM, Purwanto A, Iskandar F, Hazata M, Okuyama K. 2009. Intense UV-light absorption of ZnO nanoparticles prepared using a pulse combustion-spray pyrolysis method. Chem. Eng. J. 155(1-2):433-441. https://doi.org/10.1016/j.cej.2009.07.011

23. Lin N, Huang X, Zhang X, Fan A, Qin L, Tang B. 2012. In vitro assessments on bacterial adhesion and corrosion performance of TiN coating on Ti6Al4V titanium alloy synthesized by multi-arc ion plating. Appl. Surf. Sci. 258(18):7047-7051. https://doi.org/10.1016/j.apsusc.2012.03.163

24. Park JM, Park SJ, Kim WJ, Ghim SY. 2012. Application of antifungal CFB to increase the durability of cement mortar. J. Microbiol. Biotechnol. 22(7):1015-1020. https://doi.org/10.4014/jmb.1112.12027

25. Klienchen de Maria VP, Guedes de Paiva FF, Tamashiro JR, et al. 2024. Advances in ZnO nanoparticles in building material: Antimicrobial and photocatalytic applications – Systematic literature review. Constr. Build. Mater. 417:135337. https://doi.org/10.1016/j.conbuildmat.2024.135337

26. Adebanjo AU, Shafiq N, Kumar V, et al. 2024. Antimicrobial concrete for development: A critical review. J. Clean Prod. 458:142445. https://doi.org/10.1016/j.jclepro.2024.142445

27. Loh K, Gaylarde CC, Shirakawa MA. 2018. Photocatalytic activity of ZnO and TiO_2 'nanoparticles' for use in cement mixes. Constr. Build. Mater. 167:853-859. https://doi.org/10.1016/j.conbuildmat.2018.02.103

28. Doebelin N, Kleeberg R. 2015. Profex: a graphical user interface for the Rietveld refinement program BGMN. J. Appl. Cryst. 48(5):1573-1580. https://doi.org/10.1107/S1600576715014685

29. Dweck J, Buchler PM, Coelho ACV, Cartledge FK. 2000. Hydration of a Portland cement blended with calcium carbonate. Thermochim. Acta. 346(1-2):105-113. https://doi.org/10.1016/S0040-6031(99)00369-X

30. Lothenbach B, Durdziński P, De Weerdt K. Thermogravimetric analysis. 2016. A Practical Guide to Microstructural Analysis of Cementitious Materials. p.196-231. https://doi.org/10.1201/B19074-5

31. Hoshino S, Yamada K, Hirao H. 2006. XRD/Rietveld analysis of the hydration and strength development of slag and limestone blended cement. J. Adv. Concr. Technol. 4(3):357-367. https://doi.org/10.3151/jact.4.357

32. Mounanga P, Khelidj A, Loukili A, Baroghel-Bouny V. 2004. Predicting $Ca(OH)_2$ content and chemical shrinkage of hydrating cement pastes using analytical approach. Cem. Concr. Res. 34(2):255-265. https://doi.org/10.1016/j.cemconres.2003.07.006

33. Alizadeh R. 2009. Nanostructure and engineering properties of basic and modified calcium-silicate-hydrate systems [doctoral dissertation]. Ottawa (CA): University of Ottawa. https://doi.org/10.20381/RUOR-13206

34. Amor F, Baudys M, Racova Z, Scheinherrová L, Ingrisova L, Hajek P. 2022. Contribution of TiO_2 and ZnO nanoparticles to the hydration of Portland cement and photocatalytic properties of high performance concrete. Case Stud. Constr. Mater. 16:e00965. https://doi.org/10.1016/j.cscm.2022.e00965

35. Amor F, Ingrišová L, Rácová Z, Baudys M, Hájek P. 2022. Effect of TiO_2 and ZnO powder mixtures on mechanical and photocatalytic performance of high performance concrete. Acta Polytech. CTU Proc. 33:15-19. https://doi.org/10.14311/APP.2022.33.0015

36. Wang J, Hu Z, Chen Y, et al. 2022. Effect of Ca/Si and Al/Si on micromechanical properties of C(-A)-S-H. Cem. Concr. Res. 157:106811. https://doi.org/10.1016/j.cemconres.2022.106811

37. Arliguie G, Grandet J. 1990. Influence de la composition d'un ciment Portland sur son hydration en présence de zinc. Cem. Concr. Res. 20(4):517-524. https://doi.org/10.1016/0008-8846(90)90096-G

38. Yousuf M, Mollah A, Hess TR, Tsai YN, Cocke DL. 1993. An FTIR and XPS investigations of the effects of carbonation on the solidification/stabilization of cement based systems-Portland type V with zinc. Cem. Concr. Res. 23(4):773-784. https://doi.org/10.1016/0008-8846(93)90031-4

39. Chen J, Kou SC, Poon CS. 2012. Hydration and properties of nano-TiO_2 blended cement composites. Cem. Concr. Compos. 34(5):642-649. https://doi.org/10.1016/J.CEMCONCOMP.2012.02.009

40. Du Y, Korjakins A. 2023. Synergic effects of nano additives on mechanical performance and microstructure of lightweight cement mortar. Appl. Sci. 13(8):5130. https://doi.org/10.3390/app13085130

41. Adebanjo AU, Abbas YM, Shafiq N, Khan MI, Farhan SA, Masmoudi R. 2024. Optimizing nano-TiO_2 and ZnO integration in silica-based high-performance concrete: Mechanical, durability, and photocatalysis insights for sustainable self-cleaning systems. Constr. Build. Mater. 446:138038. https://doi.org/10.1016/J.CONBUILDMAT.2024.138038

42. Lothenbach B, Scrivener K, Hooton RD. 2011. Supplementary cementitious materials. Cem. Concr. Res. 41(12):1244-1256. https://doi.org/10.1016/J.CEMCONRES.2010.12.001

43. Nonat A. 2004. The structure and stoichiometry of C-S-H. Cem. Concr. Res. 34(9):1521-1528. https://doi.org/10.1016/j.cemconres.2004.04.035

44. Alarcon-Ruiz L, Platret G, Massieu E, Ehrlacher A. 2005. The use of thermal analysis in assessing the effect of temperature on a cement paste. Cem. Concr. Res. 35(3):609-613. https://doi.org/10.1016/J.CEMCONRES.2004.06.015

45. Šiler P, Kolářová I, Novotný R, et al. 2018. Application of isothermal and isoperibolic calorimetry to assess the effect of zinc on cement hydration. J. Therm. Anal. Calorim. 133(1):27-40. https://doi.org/10.1007/S10973-017-6815-1

46. Janczarek M, Klapiszewski Ł, Jędrzejczak P, Klapiszewska I, Ślosarczyk A, Jesionowski T. 2021. Progress of functionalized TiO_2-based nanomaterials in the construction industry: A comprehensive review. Chem. Eng. J. 430(3):132062. https://doi.org/10.1016/J.CEJ.2021.132062

47. Reches Y, Thomson K, Helbing M, Kosson DS, Sanchez F. 2018. Agglomeration and reactivity of nanoparticles of SiO_2, TiO_2, Al_2O_3, Fe_2O_3, and clays in cement pastes and effects on compressive strength at ambient and elevated temperatures. Constr. Build. Mater. 167:860-873. https://doi.org/10.1016/J.CONBUILDMAT.2018.02.032

48. Khanna S, Paneliya S, Hinshu H, et al. 2021. Incorporation of Anatase-TiO_2 in cement to enhance the self-cleaning and mechanical properties: A systematic study. Mater. Today Proc. 47(2):533-538. https://doi.org/10.1016/J.MATPR.2020.10.625

49. Amor F, Diouri A, Boukhari A. 2018. Mineralogy of C-S-H belite hydrates incorporating Zn-Al-Ti layered double hydroxides. In: MATEC Web of Conferences. 149:01020. https://doi.org/10.1051/matecconf/201714901020

50. Amor F, Diouri A, Bouregba A, Hajek P. 2022. Structural description of cement hydrates modified by incorporation of nanocomposites derived from lamellar double hydroxides. Mater. Today Proc. 58(4):1436-1441. https://doi.org/10.1016/J.MATPR.2022.02.465

51. Amor F, Diouri A, Ellouzi I, Ouanji F. 2018. Development of Zn-Al-Ti mixed oxides-modified cement phases for surface photocatalytic performance. Case Stud. Constr. Mater. 9:e00209. https://doi.org/10.1016/j.cscm.2018.e00209

52. Georget F, Bénier C, Wilson W, Scrivener KL. 2022. Chloride sorption by C-S-H quantified by SEM-EDX image analysis. Cem. Concr. Res. 152:106656. https://doi.org/10.1016/J.CEMCONRES.2021.106656

53. Mostafa FEZM, Smarzewski P, El Hafez GMA, et al. 2023. Analyzing the effects of nano-titanium dioxide and nano-zinc oxide nanoparticles on the mechanical and durability properties of self-cleaning concrete. Materials 16(21):6909. https://doi.org/10.3390/MA16216909

54. Senff L, Tobaldi DM, Lemes-Rachadel P, Labrincha JA, Hotza D. 2014. The influence of TiO_2 and ZnO powder mixtures on photocatalytic activity and rheological behavior of cement pastes. Constr. Build. Mater. 65:191-200. https://doi.org/10.1016/j.conbuildmat.2014.04.121

55. Duque-Redondo E, Bonnaud PA, Manzano H. 2022. A comprehensive review of C-S-H empirical and computational models, their applications, and practical aspects. Cem. Concr. Res. 156:106784. https://doi.org/10.1016/J.CEMCONRES.2022.106784

56. Kirkpatrick RJ, Yarger JL, McMillan PF, Ping Y, Cong X. 1997. Raman spectroscopy of C-S-H, tobermorite, and jennite. Adv. Cem. Based Mater. 5(3-4):93-99. https://doi.org/10.1016/S1065-7355(97)00001-1

57. Hong SY, Glasser FP. 1999. Alkali binding in cement pastes: Part I. The C-S-H phase. Cem. Concr. Res. 29(12):1893-1903. https://doi.org/10.1016/S0008-8846(99)00187-8

58. Podporska-Carroll J, Panaitescu E, Quilty B, Wang L, Menon L, Pillai SC. 2015. Antimicrobial properties of highly efficient photocatalytic TiO_2 nanotubes. Appl. Catal. B: Environmental. 176-177:70-75. https://doi.org/10.1016/J.APCATB.2015.03.029

59. Hegyi A, Grebenişan E, Lăzărescu AV, Stoian V, Szilagyi H. 2021. Influence of TiO_2 nanoparticles on the resistance of cementitious composite materials to the action of fungal species. Materials 14(16):4442. https://doi.org/10.3390/MA14164442

60. Chaudhuri A, Bhattacharyya S, Chaudhuri P, Sudarshan M, Mukherjee S. 2020. In vitro deterioration study of concrete and marble by Aspergillus tamarii. J. Build. Eng. 32:101774. https://doi.org/10.1016/J.JOBE.2020.101774

61. Reinprecht L, Iždinský J, Vidholdová Z. 2018. Biological resistance and application properties of particleboards containing nano-zinc oxide. Adv. Mater. Sci. Eng. 2018:2680121. https://doi.org/10.1155/2018/2680121

62. Singh VP, Sandeep K, Kushwaha HS, Powar S, Vaish R. 2018. Photocatalytic, hydrophobic and antimicrobial characteristics of ZnO nano needle embedded cement composites. Constr. Build. Mater. 158:285-294. https://doi.org/10.1016/J.CONBUILDMAT.2017.10.035

63. Lin PY, Huang YH, Chen JS, et al. 2024. Cost-effective microbial induced ZnO synthesis for building material: Antibacterial, photocatalytic and mechanical characteristics. Environ. Technol. Innov. 36:103762. https://doi.org/10.1016/J.ETI.2024.103762

64. Gómez-Ortíz N, De La Rosa-García S, González-Gómez W, et al. 2013. Antifungal coatings based on $Ca(OH)_2$ mixed with ZnO/TiO_2 nanomaterials for protection of limestone monuments. ACS Appl. Mater. Interfaces 5(5):1556-1565. https://doi.org/10.1021/am302783h

65. Tuntachon S, Kamwilaisak K, Somdee T, et al. 2019. Resistance to algae and fungi formation of high calcium fly ash geopolymer paste containing TiO_2. J. Build. Eng. 25:100817. https://doi.org/10.1016/J.JOBE.2019.100817

66. Rosa RH, Silva RS, Nascimento LL, Okura MH, Patrocinio AOT, Rossignolo JA. 2023. Photocatalytic and antimicrobial activity of TiO_2 films deposited on fiber-cement surfaces. Catalysts 13(5):861. https://doi.org/10.3390/CATAL13050861

67. Fernandes TR, Segorbe D, Prusky D, Di Pietro A. 2017. How alkalinization drives fungal pathogenicity. PLoS Pathog. 13(11):e1006621. https://doi.org/10.1371/JOURNAL.PPAT.1006621